Int. J. Nanosci. Nanotechnol., Vol. 16, No. 1, March 2020, pp. 1-12

High Efficiencies in Nanoscale Poly(3-Hexylthiophene)/Fullerene Solar Cells

Samira Agbolaghi[1,*] and Saleheh Abbaspoor[2]

[1]Chemical Engineering Department, Faculty of Engineering, Azarbaijan Shahid Madani University, P.O. BOX: 5375171379, Tabriz, Iran.
[2]School of Engineering, Damghan University, P.O. BOX: 36716–41167, Damghan, Iran.

(*) Corresponding author: s.agbolaghi@azaruniv.ac.ir
(Received: 29 December 2017 and Accepted: 16 October 2019)

Abstract

A modified morphology was introduced for poly(3-hexylthiophene):phenyl-C71-butyric acid methyl ester (P3HT:PC71BM) bulk heterojunction (BHJ) solar cells by thermal and solvent annealing treatments in the presence of hydrophilic-hydrophobic block copolymers. Power conversion efficiency (PCE) plummet was prohibited during both thermal and solvent treatments for all BHJ devices modified with either hydrophobic- or hydrophilic-based copolymers. It was originated from ever increasing trend of fill factor (FF) and increasing or marginally decreasing trend of short circuit current density (J_{sc}). Although PCEs were higher in untreated hydrophobic-compatibilized devices, the hydrophilic-compatibilized systems further benefited from thermal and solvent treatments. The vertical homogeneity increased for compatibilized BHJs during annealing processes, leading to very high FFs around 70%. The maximum values of Jsc and PCE for the well-controlled photovoltaic systems were 12.10 mA/cm^2 and 4.85%, respectively.

Keywords: *P3HT, PC71BM, Bulk Heterojunction, PCE, Solar Cell.*

1. INRODUCTION

The control of the active layer morphology in the bulk heterojunction (BHJ) mixtures of polymer donors and the fullerene acceptors has been considered as a vital feature. The optimum morphology generally contains two major factors comprising the molecular ordering within and the phase separation between the donor and acceptor phases. Poly(3-hexylthiophene) (P3HT) and [6,6]-phenyl-C61-butyric acid methyl ester (PCBM) solar cells have attracted a great deal of interest over the past decade [1,2] being routinely employed to produce the high efficient photovoltaic devices [3,4]. Unraveling the complex morphology of the P3HT: PCBM hybrid systems still remained a significant challenge. The incorporation of a third component including the fullerene derivatives and carbonic materials such as the carbon nanotubes (CNTs) to modify the interfaces in a binary blend provides better opportunities to achieve interesting microstructures [5–8]. To solve the morphological issues, several methodologies including employment or adjustment of cross-linkable materials [9, 10], block copolymers [11, 12], thermal and solvent annealing [13–28], microwave and electrical annealing [29, 30], mixed solvents [31,32], additives [33–39], functionalized and derivatives [40–43], molecular weight [44], regioregularity [45], active layer thickness [46] and blend composition [47–51] have been reported. Including a third component to modify the interfaces in a binary blend provides better opportunities to achieve interesting microstructures [52, 53]. Incorporating the block copolymers in the BHJ film is capable of stabilizing the device structure against the destructive thermal phase segregation as well [54, 55]. They promote the long-term thermal stability of the photovoltaic devices; however, most of

acquired power conversion efficiencies (PCEs) are poorer than or similar to that of the pristine solar cells. Furthermore, the compatibilizers have a little effect on the morphological structures before annealing [56].

In this work, we systematically studied the influence of thermal and solvent treatments on the performances of the P3HT:PCBM BHJs compatibilized by the rod (conductive)-coil (dielectric) block copolymers. The photovoltaic devices simultaneously benefited from the thermal stabilities and the high efficiencies. These systems could serve as a model to develop a comprehensive understanding of the strategies necessary for improving the performance of new emerging materials.

2. EXPERIMENTAL

The highly regioregular P3HTs (>99%) with the polydispersity index (PDI) ranged between 1.21–1.25 were synthesized using Grignard metathesis polymerization. The diblock copolymers, i.e., P3HT-*b*-PEG, P3HT-*b*-PMMA, and P3HT-*b*-PS were synthesized with Suzuki coupling and atom transfer radical polymerization (ATRP). In details, P3HT-Br was synthesized by Grignard metathesis polymerization [57]. A reactor was flushed with N_2 and charged with 2,5-dibromo-3-hexylthiophene and dried THF (30 mL). A 1 M solution of methyl magnesium bromide (MeMgBr) in THF was added, and refluxed for 2 h under a nitrogen protection. The 1,3-bis (diphenyl-lphosphino) propane nickel(II) chloride (Ni(dPPP)) in 8 mL anhydrous THF was added in one portion, and refluxing was continued for 100 min. The reaction mixture was then dropped in methanol under stirring. The precipitate was collected by filtration and washed with methanol. The crude polymer was extracted with methanol and hexanes to remove residual catalysts and short polymer chains. For functionalization of PEG (PEG-BE), PEG, 4-(4,4,5,5-tetramethyl-1, 3, 2-dioxaborolan-2-yl) benzoic acid (DBA), and anhydrous THF (60 mL) were added to a flask under nitrogen protection. After N,N-dicyclohexylcarbodiimide (DCC) and N,N-dimethylaminopyridine (DMAP) were added, and the mixture was stirred for 24 h at room temperature. The precipitation was filtered off, and then the mixture was poured into diethyl ether. Afterward, the precipitation was collected by filtration and washed with diethyl ether [58]. To a two-necked flask equipped with a stopcock were added P3HT-Br, PEG-BE, palladium-tetrakis(triphenylphosphine) ($Pd(PPh_3)_4$), and dried toluene (13 mL) under nitrogen. After that 3 M K_2CO_3 aq. (3 mL) was added, the mixture was stirred at 100 °C for 1 day. The solution was concentrated and poured into methanol to give the polymer. The polymer was extracted with methanol and acetone. Moreover, the dielectric homopolymers were separated via solvent extraction (deionized water for PEG). More details were reported in the literature [58]. Polystyrene (PS) or poly(methyl methacrylate) (PMMA) with tert-butyl ester as an end functional group (PS-tBE or PMMA-tBE) were synthesized by ATRP [59]. To this end, 2-Bromopropionic acid tert-butyl ester / styrene or methyl methacrylate /anisole /CuBr /CuBr2 /N, N', N', N'',N''-pentamethyldiethylenetriamine (PMD ETA) with a molar ratio of 1/0.07/50/1/0.05/1 were added into a flask equipped with a stopcock. The mixture was then heated for 24 h at 90 °C under nitrogen. The reaction mixture was poured into methanol to precipitate the product [60]. To prepare PS or PMMA with the end group of carboxylic acid (PS-CA or PMMA-CA), PS-tBE or PMMA-tBE/p-toluenesulfonic acid/dioxane with a molar ratio of 0.2/2/1 were placed into a flask equipped with a condenser, and the mixture was stirred for 24 h at 95 °C under nitrogen. The product was precipitated in methanol [60]. To prepare PS or PMMA with the end group of boronic acid ester (PS-BAE or PMMA-BAE), PS-CA or

PMMA-CA/4-(4,4,5,5-tetramethyl-1,3,2-dioxaborolan-2-yl) phenol /dicyclo-hexylcarbo diimide/ N, N-dimethy-laminopyridine with a molar ratio of 0.33/1.17/1/1 were added into a flask having CH2Cl2 (5 mL), then the mixture was stirred for 24 h at room temperature under nitrogen. After reaction a few drops of water was added. Precipitate was removed by filtration and the product was precipitated in methanol [60]. To synthesize P3HT-*b*-PS and P3HT-*b*-PMMA block copolymers, $Pd(PPh_3)_4$, 3 M K_2CO_3 (aqueous solution, 0.35 ml), PS-BAE or PMMA-BAE, P3HT-Br, and toluene (7 mL) were placed into a flask equipped with a condenser. Then the mixture was stirred for 24 h at 100 °C. The product was precipitated in methanol and acetone [60]. Furthermore, the dielectric homopolymers were separated via solvent extraction (e.g., cyclohexane for PS).

^{1}HNMR spectra of various synthesized polymers are displayed in Figure 1. In ^{1}HNMR spectrum of P3HT-*b*-PS block copolymers, the signals in aromatic region assignable to the protons on the phenyl ring of PS could be observed at 7.1 and 6.6 ppm [60].

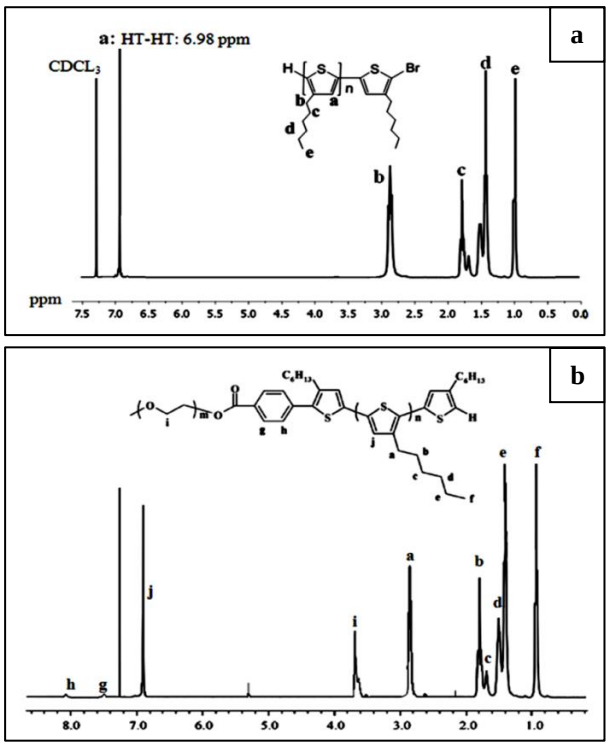

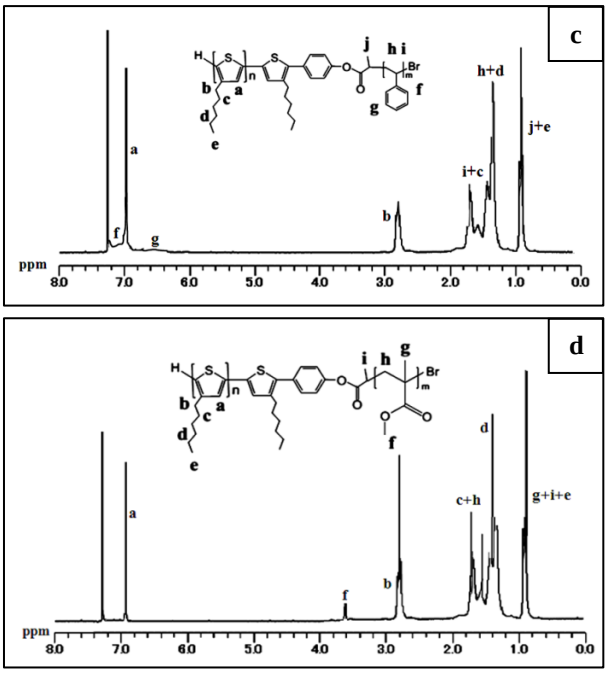

Figure 1. *^{1}HNMR spectra of synthesized P3HT$_{4880}$0-Br homopolymers (a) as well as P3HT$_{21000}$-b-PEG$_{750}$ (b), P3HT$_{7150}$-b-PS$_{519}$ (c), and P3HT$_{21000}$-b-PMMA$_{497}$ (c) block copolymers.*

The signal appeared at 3.60–3.65 ppm was also indicative of methyl methacrylate polymerization during ATRP [61]. In addition, the disappearance of the small triplet signal at 2.56 ppm was observed, which was assigned as the signal of methylene proton on the first carbon of hexyl group substituted on the bromo-terminal unit [62]. In the ^{1}HNMR spectrum of P3HT-*b*-PEG, the signal assignable to PEG was observed at 3.7 ppm. The protons of the phenyl at 8.1 ppm and 7.5 ppm indicated that the terminal thiophene unit was successfully substituted by PEG segment in Suzuki coupling [58]. The respective signals of hexyl side chains also appeared at 0.8–1.8 ppm [58].

The ternary blend solutions of the P3HT: PCBM (purity >99%):compatibilizer were spin-coated inside a nitrogen glove box onto poly(3,4-ethylenedioxythiophene): poly(styrene sulfonate) (PEDOT:PSS) modified ITO on the glass to yield 150 nm films. The weight ratio of P3HT:PCBM was 1:1.5 wt/wt and the P3HT-*b*-PS, P3HT-*b*-PMMA, and P3HT-*b*-PEG$_{750}$

were dissolved at different ratios in 1,2-dichlorobenzene (ODCB) with a total concentration of 20 mg/ml. The solvent and thermal annealing processes were conducted at room temperature (in a glass Petri dish covered with a glass cap) and 150 °C (on a temperature controlled hot plate), respectively. The samples were then kept at room temperature in a N_2-filled glove box before analyzing. Then, a thin LiF interfacial layer (ca. 1 nm) and a 100 nm film of Al were thermally evaporated onto the device under a high vacuum (base pressure less than 2×10^{-4} Pa).

3. RESULTS AND DISCUSSION

3.1. Crystallization and Morphology

The two dimensional grazing incidence wide angle X-ray scattering (2D GIWAXS) profile of a typical active layer is depicted in Figure 2(a). The orientation and fabricating planes are also displayed in Figure 2(b).

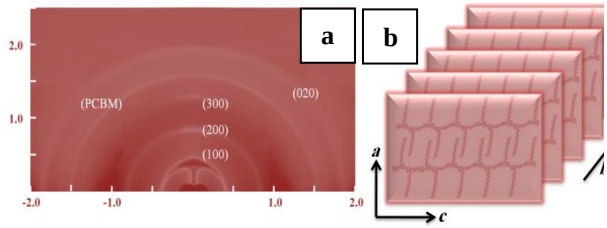

Figure 2. *(a) 2D GIWAXS profile of a spin-coated active layer based on P3HT and PC71BM; (b) the scheme of edge-on oriented P3HT crystals and fabricating planes.*

In the presence of $P3HT_{7150}$-*b*-PEG copolymers, the external treatments resulted in a higher phase separation between donor and acceptor components compared to BHJs modified by $P3HT_{7150}$-*b*-PS and $P3HT_{7150}$-*b*-PMMA. Figures 3(a-i) represent energy filtered transmission electron microscopy (EFTEM) images for the untreated and treated active layers. The hydrophobic-based compatibilizers prevented the donor and acceptor domains from extremely coarsening during annealing (Figures 3(d-f)). During thermal and solvent treatments, the P3HT crystallite sizes had an increasing trend. The coarsening slope for the P3HT crystallites in P3HT-*b*-PS and P3HT-*b*-PMMA compatibilized systems decreased versus the annealing time. The P3HT crystallites grew faster in the shorter periods of time, thereby by annealing processes, the rate of the crystallite growth reduced. A similar phenomenon occurred during the solvent annealing. In the BHJ systems compatibilized with P3HT-*b*-PS and P3HT-*b*-PMMA block copolymers, within the shorter periods of annealing time, the P3HT crystallite sizes were almost larger in the thermal annealed films compared to those detected for the solvent annealed ones. It was assigned to the higher mobility of the P3HT chains at elevated temperature (150 °C) during the thermal annealing, reflecting the larger P3HT crystallites within the similar annealing times. After a given annealing time, the P3HT crystallites were larger in the solvent annealing within the similar annealing time. In longer periods of the annealing time in both solvent and thermal annealed systems, the P3HT crystallites reached a marginally saturated state. Here, this was the thermodynamics which controlled the system, and facilitated further growth of the P3HT crystallites; whereas in P3HT-*b*-PEG modified systems, always the influence of the thermal annealing on the P3HT crystallites was more conspicuous compared to the solvent annealing. The thermal annealing as a fast growth treatment provided a driving force better than the solvent annealing as a slow growth treatment.

The P3HT crystallite size versus the thermal and solvent annealing time is reported in Figures 4(a) and (b). Coarsening slopes of P3HT crystallites during annealing processes were steeper for the hydrophilic - compatibilized systems. Indeed, in the hydrophobic - compatibilized systems, the P3HT crystallites demonstrated a higher resistance against coarsening during annealing processes, and thus their coarsening slope versus the annealing time was lower. Furthermore, this resistance against coarsening of the P3HT crystallites was intensified by further passing the annealing time. This could be attributed to the coherent BHJ network and dense P3HT crystallites in the presence of the hydrophobic based block copolymers.

However, coarsening in the P3HT crystallites versus the annealing time for P3HT-*b*-PEG compatibilized systems strongly continued even in the longer periods of the annealing time (Figures 4(a) and (b)).

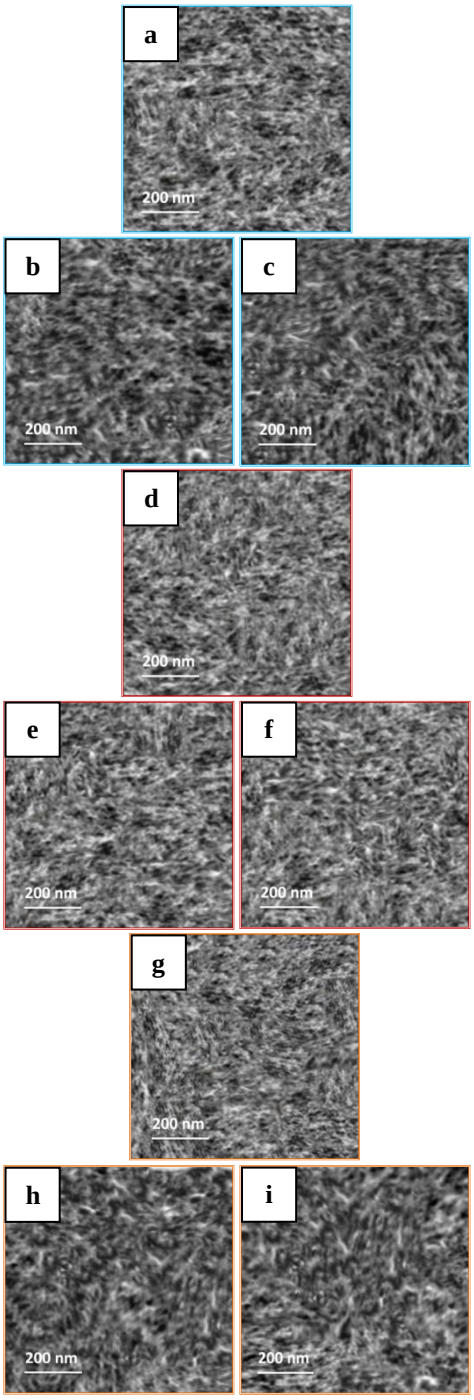

Figure 3. *EFTEM images of uncompatibilized (a-c) and compatibilized active layers by 30 wt% of P3HT$_{7150}$-b-PS (d-f) and P3HT$_{7150}$-b-PEG (g-i) block copolymers. Morphologies represent the untreated BHJs ((a), (d), and (g)) and the thermal (150 °C) ((b), (e), and (h)) and solvent (25 °C) ((c), (f), and (i)) annealed systems for 120 min.*

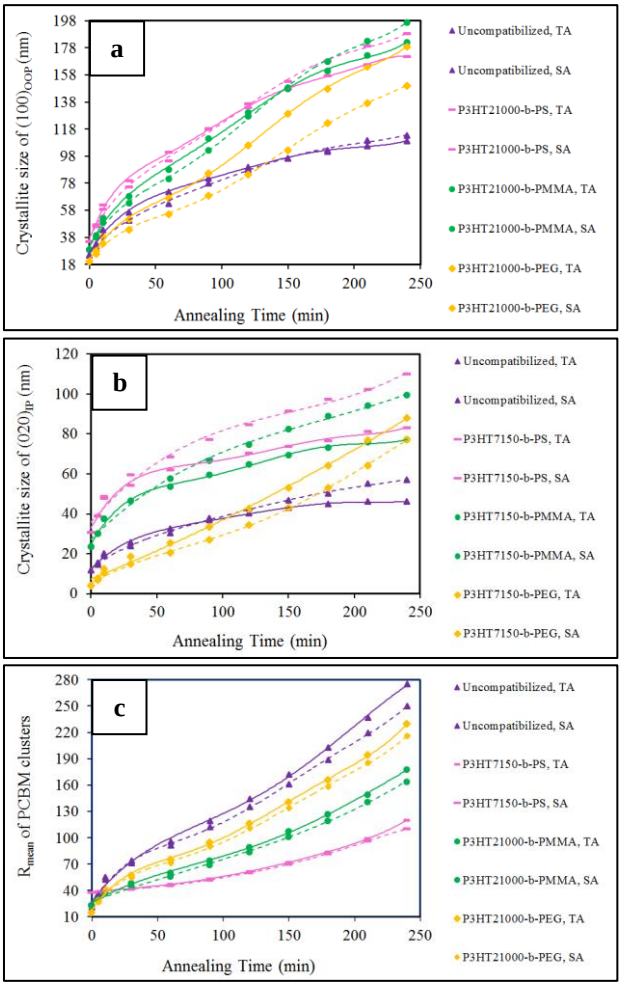

Figure 4. *The P3HT crystallite sizes versus the annealing time in (100)$_{OOP}$ (a) and (020)$_{IP}$ (b) directions and the PCBM cluster sizes (c) for various uncompatibilized and compatibilized thin films with P3HT-b-PS, P3HT-b-PMMA, P3HT-b-PEG block copolymers during thermal and solvent annealing treatments.*

In all BHJ systems, either uncompatibilized or compatibilized, during both thermal and solvent annealing processes, *d*-spacing depicted an ever soaring trend. The distances between the crystallographic planes were calculated from (100)$_{OOP}$ and (020)$_{IP}$ Bragg peaks position for the edge-on (with the alkyl chain perpendicular to the substrate) and from (100)$_{IP}$ and (020)$_{OOP}$ Bragg peaks position for the face-on (with the alkyl chain parallel with the substrate) P3HT crystallites. The

increasing slope of *d*-spacing in $(100)_{OOP}$ direction during thermal annealing was significantly steeper than that detected under the solvent annealing. Actually, the high-temperature (150 °C) thermal annealing further loosened the P3HT crystallites. Before conducting the treatments, *d*-spacings for the hydrophobic-compatibilized BHJs were considerably lower. This resistance against loosening of the P3HT crystallites was also detected during the thermal annealing. Although there was a significant difference between the thermal and solvent annealing treatments on *d*-spacing enhancement in $(100)_{OOP}$ direction of the P3HT crystallites, in $(020)_{IP}$ or π-π stacking direction, an infinitesimal distinct was detected. More explanations are represented in Supplementary.

During annealing processes, coarsening also occurred in the PCBM clusters but with various slopes. Guinier approximation was used to determine mean PCBM cluster size (R_{mean}) from the low-Q scattering range (ca. 0.006–0.012 $Å^{-1}$) of the GISAXS curves. Similar to the literature [63], in this work the PCBM scattering intensity increased as a result of forming the larger PCBM clusters. Coarsening versus the annealing time in the uncompatibilized systems was the highest as shown in Figure 4(c), because, P3HT:PC71BM BHJs were not resistant against coarsening during the external treatments. Among the modified systems, the steepest coarsening slope belonged to P3HT-*b*-PEG compatibilized ones. By using the block copolymers having more hydrophobic coily blocks, coarsening of the PCBM clusters versus the annealing time decreased. It could be related to the stabilization of the BHJ morphology via the hydrophobic based compatibilizers, and subsequent increase of their resistance against coarsening during annealing processes. Before conducting any treatment, in P3HT-*b*-PEG compatibilized systems, the PCBM cluster sizes were the smallest among all BHJs. Smaller PCBM clusters before annealing showed a higher tendency and potential for coarsening under the external treatments. In parallel with the PCBM clusters coarsening, the weakened fluorescence quenching suggested decreased interface area. The cluster coarsening assisted the charge collection through the formation of a network for the efficient electron transport, thus preventing losses due to bimolecular recombination. Moreover, the coherent networking in the hydrophilic-compatibilized systems resulted in a slower PCBM cluster coarsening during treatments compared to the uncompati-bilized BHJ. Coarsening slope was also steeper in P3HT-*b*-PMMA compatibilized films than P3HT-*b*-PS modified ones (Figure 4(c)). By increasing the hydrophobicity of the coily blocks, they could further inhibit the cluster coarsening. They did this task by surrounding the PCBM clusters and inducing a higher order and coherency to the BHJ systems.

Similar to the P3HT crystallites, in the PCBM clusters, *d*-spacing between the PCBM molecules increased during both thermal and solvent treatments. The *d*-spacings of PCBM molecules inside the PCBM clusters were calculated based on the peak center position of the PCBM clusters appeared in GIWAXS graphs. The *d*-spacing enhancement of the PCBM molecules in respective clusters was milder under the slow growth annealing compared to the fast growth treatment. Furthermore, the slope of *d*-spacing increase in the BHJs compatibilized with the block copolymers having more hydrophobic coily blocks was lower. In fact, the hydrophobic coily blocks not only prevented the PCBM clusters from coarsening during annealing processes but also largely prohibited their loosening.

3.2. Photovoltaic Characteristics of Modified devices

In this section, the device performances correlate with the BHJ morphologies modified by the rod-coil block copolymers under thermal and solvent treatments. The increased *PCE*s, combined with a good thermal stability of devices using the block copolymer compatibilizers, indicated their promising potential for the polymer solar cell applications. The best photovoltaic characteristics, i.e., *PCE* (4.85%), J_{sc} (12.10 mA/cm^2), *FF* (69%) and V_{oc} (0.60 V) were obtained thanks to the nanoscale morphology promotion in the active layers. Some *J-V* curves for the uncompatibilized and compatibilized systems with various compatibilizers and treated under thermal and solvent annealing processes are reported in Figures 6(a-d). Notably, even after long-term treatments, the *PCE*s were

high. Therefore, the conspicuous enhancement in the *PCE*s during the annealing processes originated from the rod-coil block copolymer compatibilizers. In Figure 6(a), the variation of the *PCE*s versus the annealing time is reported for some uncompatibilized and compatibilized BHJs by P3HT$_{7150}$-*b*-PS, P3HT$_{7150}$-*b*-PMMA, and P3HT$_{7150}$-*b*-PEG block copolymers. By further conducting the thermal and solvent annealing processes, the *PCE*s considerably dropped for the uncompatibilized photovoltaic cells. The *PCE* for these systems reached from 1.65% to 2.14% within 60 min of thermal annealing and then plummeted to 0.18% after 240 min. The *PCE* decrease was rather low for the solvent annealed uncompatibilized systems. The *PCE* of this device treated under solvent annealing peaked at 2.41% after 90 min and then reduced to 0.63% within 240 min.

In the photovoltaic devices compatibilized by P3HT-*b*-PS, P3HT-*b*-PMMA, and P3HT-*b*-PEG block copolymers, various behaviors were detected for the *PCE* alteration during solvent and thermal treatments. As illustrated in Figure 6(a), in the presence of P3HT$_{7150}$-*b*-PS block copolymers, the *PCE* was 4.07% before any treatment. By conducting the thermal annealing for 10 min, *PCE* peaked at 4.78%. Through further treating, the *PCE* reached somehow its primary value (= 4.08%) within 120 min. Finally, within 240 min, the *PCE* decreased to 3.42%. It is vital to mention that in the compatibilized system with P3HT$_{7150}$-*b*-PMMA block copolymers, after 240 min under both thermal (= 3.56%) and solvent (= 3.51%) treatments, the *PCE*s were greater than the corresponding *PCE* before external treating (= 3.13%). On the other hand, in the presence of P3HT$_{7150}$-*b*-PEG block copolymers during both thermal and solvent annealing processes, the *PCE* depicted an ever soaring trend (Figure 6(a)). For example, the *PCE* in the presence of P3HT$_{21000}$-*b*-PEG block copolymers (= 2.35%) after 60, 150, and 210 min of the thermal annealing reached 3.14, 3.70, and 3.87%, respectively, and within the similar times of the solvent annealing obtained the values of 3.29, 3.73, and 3.89%, respectively.

Although before treatments, the *PCE*s were higher in the hydrophobic-compatibilized devices, the hydrophilic-compatibilized systems further benefited from the thermal and solvent annealing processes. The *PCE*s of the latter photovoltaic cells not only did not drop but also showed an ever increasing trend during the external treatments. The principal reason for this phenomenon was related to variations of J_{sc} (Figure 6(b)) and *FF* (Figure 6(c)) during the treatments. These two parameters (J_{sc} and *FF*) aided the photovoltaic functions to be more stabilized during the annealing processes. Even if one of them dropped the other compensated it.

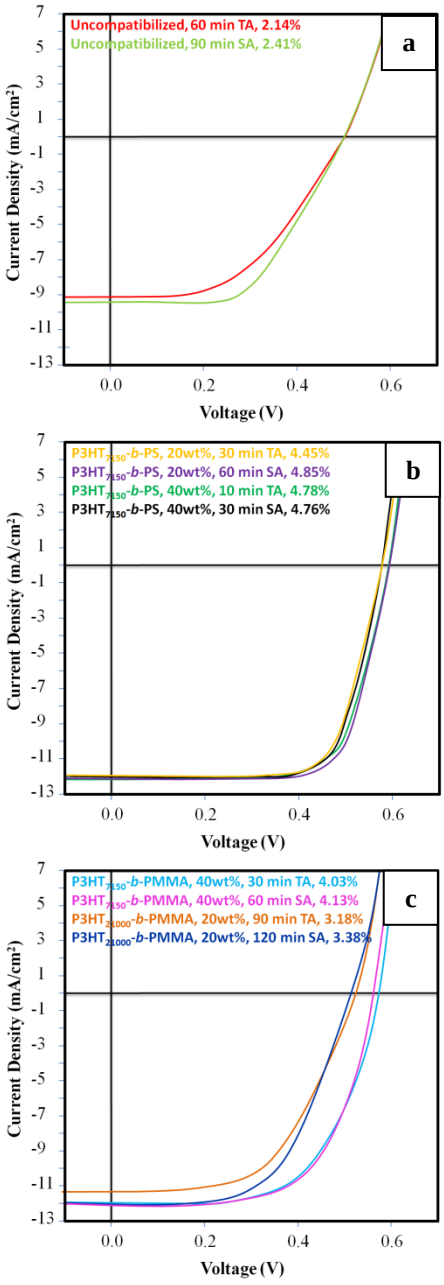

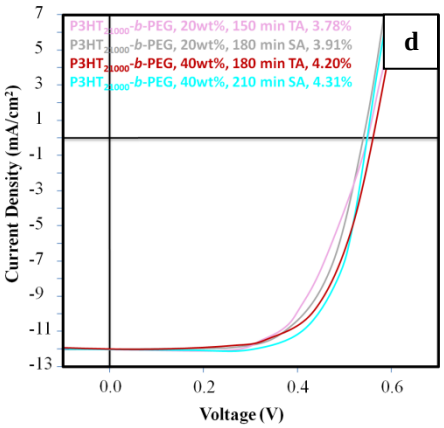

Figure 5. *J–V curves of some photovoltaic devices with uncompatibilized (a) and compatibilized active layers using P3HT-b-PS (b), P3HT-b-PMMA (c), P3HT-b-PEG (d).*

The P3HT-b-PS and P3HT-b-PMMA block copolymers largely prevented J_{SC} from sharply decrease during annealing processes, especially under solvent annealing (Figure 6(b)).

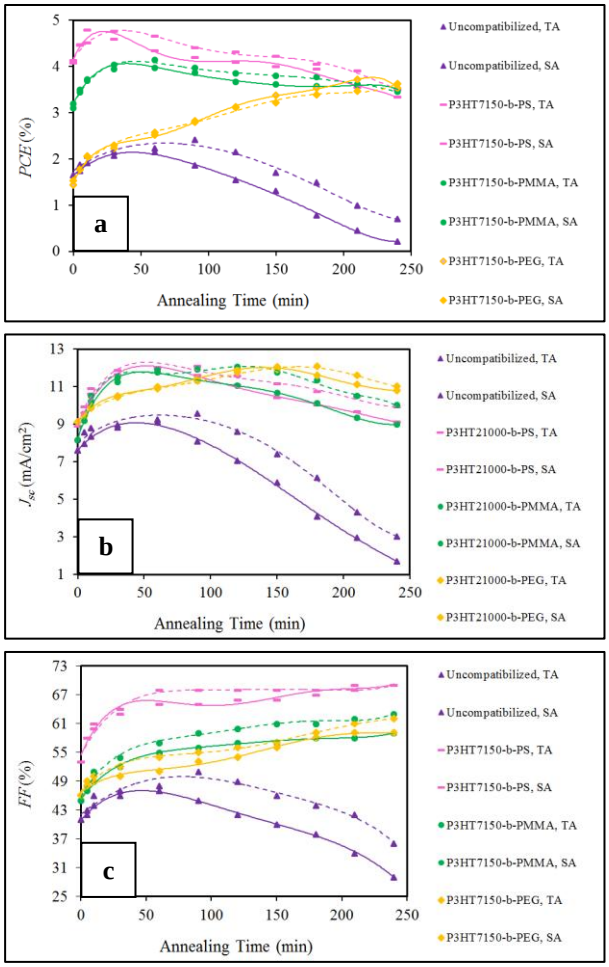

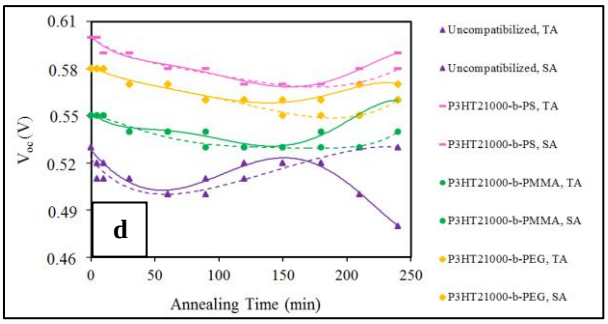

Figure 6. *Characteristics of the photovoltaic cells including PCE (a), J_{SC} (b), FF (c) and V_{OC} (d) versus the annealing time in the presence of P3HT-b-PS, P3HT-b-PMMA, P3HT-b-PEG compatibilizers during thermal and solvent treatments.*

In general, the resistance against the *PCE* dropping during both thermal and solvent treatments was detected for all BHJ devices compatibilized with the hydrophobic and hydrophilic based block copolymers. It was assigned to ever increasing trend of *FF* as well as increasing or marginally decreasing trend of J_{SC} originated from various conditions in distinct BHJ systems. In long-term annealing time, V_{OC} enhancement participated in stabilizing the *PCE* as well (Figure 6(d))). In the BHJ active layers compatibilized with the block copolymers having the hydrophobic coily blocks, due to stabilization of the morphology, extremely coarsening of the PCBM clusters during the annealing processes was significantly prohibited. The hydrophobic based rod-coil block copolymers did the modification and stabilization tasks by surrounding the donor and acceptor domains. In contrast, in the thin films compatibilized by the block copolymers having the hydrophilic coily blocks, coarsening of the PCBM clusters during annealing processes was conspicuously higher. Instead, during the annealing processes the crystallinity of these BHJs considerably increased even above the crystallinity of the hydrophobic-compatibilized systems. The crystallinity enhancement influenced the hole mobility, J_{SC}, and *FF*. Moreover, the P3HT crystallites in the presence of the hydrophilic based compatibilizers, which were even smaller than those in the uncompatibilized BHJs, grew intensively during annealing processes. The P3HT crystallite sizes were comparable for the

hydrophilic- and hydrophobic –compatibilized systems under similar external treatments. This in turn promoted the photovoltaic characteristics of the devices whose active layers were modified using P3HT-*b*-PEG block copolymers during thermal and solvent annealing treatments.

A homogeneous distribution of donor and acceptor components in the vertical of the active layer during solvent and thermal annealing processes significantly improved *FF*. The hole and electron mobilities under treatments in the compatibilized BHJ thin films with either hydrophilic or hydrophobic coily blocks peaked at the maximum values. In fact, for each kind of compatibilizers and their composition, there existed an optimum morphology during solvent and thermal treatments. In the optimum morphology for each BHJ, μ_h, μ_e, J_{sc} and *PCE* were in their maximum values. In the compatibilized systems, *FF* most of the time had an increasing trend, whereas for the uncompatibilized devices, *FF* after peaking at the optimum morphology, depicted a declining trend (Figure 6(c)).

For the compatibilized active layers, the optimum morphology and the PCE_{max} acquired faster for the thermal annealing than the solvent annealing. Because the high-temperature thermal annealing (150 °C) was a fast growth condition, thereby made the BHJ system rapidly reach its best performance. Eventually, depending on the balance between the photovoltaic characteristics, the *PCE* could be higher in the optimum morphology of either solvent or thermal annealed active layers.

3. CONCLUSION

The nanostructure of the P3HT: PC71BM, which was critical for the photovoltaic device performance, was modified by conducting the thermal and solvent treatments in the BHJ systems compatibilized with the rod-coil block copolymer compatibilizers. In contrast to the uncompatibilized photovoltaic cells, the *PCE* did not plummet under thermal and solvent treatments for all devices compatibilized with either hydrophobic- or hydrophilic-based block copolymers. It was assigned to the compensation of J_{sc} decrease with *FF* and V_{oc} enhancement within the long-term treatments. The best photovoltaic characteristics comprising *PCE* (4.85%), J_{sc} (12.10 mA/cm^2), *FF* (69%) and V_{oc} (0.60 V) were correlated to the nanoscale morphology promotion in the active layer.

REFERENCES

1. Campoy-Quiles, M., Ferenczi, T., Agostinelli, T., Etchegoin, P. G., Kim, Y., Anthopoulous, T., Stavrinou, P. N., Bradley, D. D. C., Nelson, J., (2008). "Morphology evolution via self-organization and lateral and vertical diffusion in polymer:fullerene solar cell blends", *Nat. Mat.,* 7: 158-164.
2. Guo, T. F., Wen, T. C., L′Vovich Pakhomov, G., Chin, X. G., Liou, S.-H., Yeh, P. H., Yang, C. H., (2008). "Effects of film treatment on the performance of poly (3-hexylthiophene)/soluble fullerene-based organic solar cells", *Thin Solid Films,* 516: 3138-3142.
3. Wu, J. L., Chen, F. C., Hsiao, Y. S., Chien, F. C., Chen, P., Kuo, C. H., Huang, M. H., Hsu, C. S., (2011). "Surface plasmonic effects of metallic nanoparticles on the performance of polymer bulk heterojunction solar cells", *ACS Nano,* 5: 959-967.
4. Guo, X., Cui, C. H., Zhang, M. J., Huo, L. J., Huang, Y., Hou, J. H., Li, Y. F., (2012). "High efficiency polymer solar cells based on poly(3-hexylthiophene)/indene-C70 bisadduct with solvent additive", *Energy Environ. Sci.,* 5: 7943-7949.
5. Washburn, N. R., Lodge, T. P., Bates, F. S., (2000). "Ternary polymer blends as model surfactant systems", *J. Phys. Chem. B,* 104: 6987-6997.
6. Vahidipour, M., Vakili-Nezhaad, G., (2010). "Application of parametric L-systems to generate the figures of two series of spherical fullerenes", *Int. J. Nanosci. Nanotechnol.,* 6: 71-77.
7. Shojaosadati, S. A., Ganji, F., Zahedi, B., Rafiee-pour, H. A., Ghourchian, H., (2010). "Effect of different CNT's oxidation methods on thiocoline detection by surfactant modified graphite electrodes", *Int. J. Nanosci. Nanotechnol.,* 6: 195-204.
8. Ghozatloo, A., Yazdani, A., Shariaty-Niassar, M., (2017). "Morphology change and structural evaluation of carbon nanostructures", *Int. J. Nanosci. Nanotechnol.,* 13: 97-104.
9. Miyanishi, S., Tajima, K., Hashimoto, K., (2009). "Morphological stabilization of polymer photovoltaic cells by using cross-linkable poly (3-(5-hexenyl) thiophene)", *Macromolecules,* 42: 1610-1618.

10. Ouhib, F., Tomassetti, M., Manca, J., Piersimoni, F., Spoltore, D., Bertho, S., Moons, H., Lazzaroni, R., Desbief, S., Jerome, C., Detrembleur, C., (2013). "Thermally stable bulk heterojunction solar cells based on cross-linkable acrylate-functionalized polythiophene diblock copolymers", *Macromolecules,* 46: 785-795.
11. Miyanishi, S., Zhang, Y., Tajima, K., Hashimoto, K., (2010). "Fullerene attached all-semiconducting diblock copolymers for stable single-component polymer solar cells", *Chem. Commun.,* 46: 6723-6725.
12. Lee, J. U., Cirpan, A., Emrick, T., Russell, T. P., Jo, W. H., (2009). "Synthesis and photophysical property of well-defined donor–acceptor diblock copolymer based on regioregular poly(3-hexylthiophene) and fullerene", *J. Mater. Chem.,* 19: 1483-1489.
13. Huang, Y. C., Chia, H. C., Chuang, C. M., Tsao, C. S., Chen, C. Y., Su, W. F., (2013). "Facile hot solvent vapor annealing for high performance polymer solar cell using spray process", *Sol. Energy Mater. Sol. Cells,* 114: 24-30.
14. Kim, K. J., Bae, J. J., Seo, Y. S., Kang, B. H., Yeom, S. H., Kwon, D. H., Kang, S. W., (2012). "Enhancement of Active Layer Characteristics with Solvent Spray Annealing Treatment for Organic Solar Cell", *Jpn. J. Appl. Phys.,* 51: 088003.
15. Chen, D., Nakahara, A., Wei, D., Nordlund, D., Russell, T. P., (2010). "P3HT/PCBM bulk heterojunction organic photovoltaics: correlating efficiency and morphology", *Nano Lett.,* 11: 561-567.
16. Wu, W. R., Jeng, U. S., Su, C. J., Wei, K. H., Su, M. S., Chiu, M. Y., Chen, C. Y., Su, W. B., Su, C. H., Su, A. C., (2011). "Competition between fullerene aggregation and poly (3-hexylthiophene) crystallization upon annealing of bulk heterojunction solar cells", *ACS Nano,* 5: 6233-6243.
17. Lin, X., Seok, J., Yoon, S., Kim, T., Kim, B. S., Kim, K., (2014). "Morphological investigation of P3HT/PCBM heterojunction and its effects on the performance of bilayer organic solar cells", *Synth. Met.,* 196: 145-150.
18. Han, B., Gopalan, S. A., Lee, K. D., Kang, B. H.; Lee, S. W., Lee, J. S., Kwon, D. H., Lee, S. H., Kang, S. W., (2014). "Preheated solvent exposure on P3HT: PCBM thin film: A facile strategy to enhance performance in bulk heterojunction photovoltaic cells", *Curr. Appl. Phys.,* 14: 1443-1450.
19. Veerender, P., Saxena, V., Chauhan, A. K., Koiry, S. P., Jha, P., Gusain, A., Choudhury, S., Aswal, D. K., Gupta, S. K., (2014). "Probing the annealing induced molecular ordering in bulk heterojunction polymer solar cells using in-situ Raman spectroscopy", *Sol. Energy Mater. Sol. Cells,* 120: 526-535.
20. Shen, H., Zhang, W., Mackay, M. E., (2014). "Dual length morphological model for bulk-heterojunction, polymer-based solar cells", *J. Polym. Sci., Polym. Phys.,* 52: 387-396.
21. Wang, H., Zheng, Y., Zhang, L., Yu, J., (2014). "Effect of two-step annealing on the performance of ternary polymer solar cells based on P3HT: PC 71 BM: SQ", *Sol. Energy Mater. Sol. Cells,* 128: 215-220.
22. Aloui, W., Adhikari, T., Nunzi, J. M., Bouazizi, A., (2016). "Effect of thermal annealing on the structural, optical and dielectrical properties of P3HT:PC70BM nanocomposites", *Mater. Res. Bull.,* 78: 141-147.
23. Jung, B., Kim, K., Eom, Y., Kim, W., (2015). "High-pressure solvent vapor annealing with a benign solvent to rapidly enhance the performance of organic photovoltaics", *ACS Appl. Mater. Interfaces,* 7: 13342-13349.
24. Aziz, F., Ismail, A. F., Aziz, M., Soga, T., (2014). "Effect of solvent annealing on the crystallinity of spray coated ternary blend films prepared using low boiling point solvents", *Chem. Eng. Process.,* 79: 48-55.
25. Liao, H. C., Tsao, C. S., Huang, Y. C., Jao, M. H., Tien, K. Y., Chuang, C. M., Chen, C. Y., Su, C. J., Jeng, U. S., Chend, Y. F., Su, W. F., (2014). "Insights into solvent vapor annealing on the performance of bulk heterojunction solar cells by a quantitative nanomorphology study", *RSC Adv.,* 4: 6246-6253.
26. Fu, C. M., Jeng, K. S., Li, Y. H., Hsu, Y. C., Chi, M. H., Jian, W. B., Chen, J. T., (2015). "Effects of thermal annealing and solvent annealing on the morphologies and properties of poly(3-hexylthiophene) nanowires", *Macromol. Chem. Phys.,* 216: 59-68.
27. Gupta, S. K., Jindal, R., Garg, A., (2015). "Microscopic investigations into the effect of surface treatment of cathode and electron transport layer on the performance of inverted organic solar cells", *ACS Appl. Mater. Interfaces,* 7: 16418-16427.
28. Huang, W., Gann, E., Cheng, Y. B., McNeill, C. R., (2015). "In-depth understanding of the morphology–performance relationship in polymer solar cells", *ACS Appl. Mater. Interfaces,* 7: 14026-14034.
29. Padinger, F., Rittberger, R. S., Sariciftci, N. S., (2003). "Effects of postproduction treatment on plastic solar cells", *Adv. Funct. Mater.,* 13: 85-88.
30. Ko, C. J., Lin, Y. K., Chen, F. C., (2007). "Microwave annealing of polymer photovoltaic devices", *Adv. Mater.,* 19: 3520-3523.
31. Xiao, Y., Zhou, S., Su, Y., Wang, H., Ye, L., Tsang, S. W., Xie, F., Xu, J., (2014). "Enhanced efficiency of organic solar cells by mixed orthogonal solvents", *Org. Electron.,* 15: 2007-2013.
32. Hernandez, J. L., Reichmanis, E., Reynolds. J. R., (2015). "Probing film solidification dynamics in polymer photovoltaics", *Org. Electron.,* 25: 57-65.
33. Mohammadi-Arbati, E., Agbolaghi, S., (2019). "Efficiency above 6% in poly (3-hexylthiophene): phenyl-C-butyric acid methyl ester photovoltaics via simultaneous addition of poly (3-hexylthiophene) based grafted graphene nanosheets and hydrophobic block copolymers", *Polym. Int.,* 68: 1292-1302.

34. Agbolaghi, S., Aghapour, S., Charoughchi, S., Abbasi, F., Sarvari, R., (2018). "High-performance photovoltaics by double-charge transporters using graphenic nanosheets and triisopropylsilylethynyl/naphthothiadiazole moieties", *J. Ind. Eng. Chem.*, 68: 293-300.
35. Dang, M. T., Hirsch, L., Wantz, G., Wuest, J. D., (2013). "Controlling the morphology and performance of bulk heterojunctions in solar cells. Lessons learned from the benchmark poly (3-hexylthiophene):[6, 6]-phenyl-C61-butyric acid methyl ester system", *Chem. Rev.*, 113: 3734-3765.
36. Salim, T., Wong, L. H., Bräuer, B., Kukreja, R., Foo, Y. L., Bao, Z., Lam, Y. M., (2011). "Solvent additives and their effects on blend morphologies of bulk heterojunctions", *J. Mater. Chem.*, 21: 242-250.
37. Zeighami, M., Agbolaghi, S., Hamdast, A., Sarvari, R., (2019). "Graphenic nanosheets sandwiched between crystalline cakes of poly (3-hexylthiophene) via simultaneous grafting/crystallization and their applications in active photovoltaic layers", *J. Mater. Sci.: Mater. Electron.*, 30: 7018-7030.
38. Zhang, Y., Li, Z., Wakim, S., Alem, S., Tsang, S. W., Lu, J., Ding, J., Tao, Y., (2011). "Bulk heterojunction solar cells based on a new low-band-gap polymer: morphology and performance", *Org. Electron.*, 12: 1211-1215.
39. Agbolaghi, S., Abbaspoor, S., Abbasi, F., (2016). "Detection of polymer brushes developed via single crystal growth", *Int. J. Nanosci. Nanotechnol.*, 12: 79-90.
40. Chen, C. M., Jen, T. H., Chen, S. A., (2015). "Effective end group modification of poly (3-hexylthiophene) with functional electron-deficient moieties for performance improvement in polymer solar cell", *ACS Appl. Mater. Interfaces*, 7: 20548-20555.
41. Agbolaghi, S., Charoughchi, S., Aghapour, S., Abbasi, F., Bahadori, A., Sarvari, R., (2018). "Bulk heterojunction photovoltaics with improved efficiencies using stem-leaf, shish-kebab and double-fibrillar nano-hybrids based on modified carbon nanotubes and poly (3-hexylthiophene)", *Sol. Energy*, 170: 138-150.
42. Sakthivel, P., Kranthiraja, K., Saravanan, C., Gunasekar, K., Kim, H. I., Shin, W. S., Jeong, J. E., Woo, H. Y., Jin, S. H., (2014). "Carbazole linked phenylquinoline-based fullerene derivatives as acceptors for bulk heterojunction polymer solar cells: effect of interfacial contacts on device performance", *J. Mater. Chem. A*, 2: 6916-6921.
43. Hamdast, A., Agbolaghi, S., Zeighami, M., Beygi-Khosrowshahi, Y., Sarvari, R., (2019). "Butterfly nanostructures via regioregularly grafted multi-walled carbon nanotubes and poly (3-hexylthiophene) to improve photovoltaic characteristics", *Polym. Int.*, 68: pp.335-343.
44. Tzabari, L., Wang, J., Lee, Y. J., Hsu, J. W., Tessler, N., (2014). "Role of charge transfer states in P3ht-fullerene solar cells", *J. Phys. Chem. C*, 118: 27681-27689.
45. Guilbert, A. A. Y., Schmidt, M., Bruno, A., Yao, J., King, S., Tuladhar, S. M., Kirchartz, T., Alonso, M. I., Goñi, A. R., Stingelin, N., Haque, S. A., Campoy-Quiles, M., Nelson, J., (2014). "Spectroscopic evaluation of mixing and crystallinity of fullerenes in bulk heterojunctions", *Adv. Funct. Mater.*, 24: 6972-6980.
46. Movla, H., Mohammadalizad Rafi, A., Mohammadalizad Rafi, N., (2015). "A model for studying the performance of P3HT: PCBM organic bulk heterojunction solar cells", *Optik*, 126: 1429-1432.
47. Dang, M. T., Wantz, G., Bejbouji, H., Urien, M., Dautel, O. J., Vignau, L., Hirsch, L., (2011). "Polymeric solar cells based on P3HT: PCBM: Role of the casting solvent", *Sol. Energy Mater. Sol. Cells*, 95: 3408-3418.
48. van Bavel, S. S., Bärenklau, M., de With, G., Hoppe, H., Loos, J., (2010). "P3HT/PCBM bulk heterojunction solar cells: impact of blend composition and 3D morphology on device performance", *Adv. Funct. Mater.*, 20: 1458-1463.
49. Radbeh, R., Parbaile, E., Bouclé, J., Di Bin, C., Moliton, A., Coudert, V., Rossignol, F., Ratier, B., (2010). "Nanoscale control of the network morphology of high efficiency polymer fullerene solar cells by the use of high material concentration in the liquid phase", *Nanotechnology*, 21: 035201.
50. Vakhshouri, K., Kesava, S. V., Kozub, D. R., Gomez, E. D., (2013). "Characterization of the mesoscopic structure in the photoactive layer of organic solar cells: A focused review", *Mater. Lett.*, 90: 97-102.
51. Holmes, N. P., Nicolaidis, N., Feron, K., Barr, M., Burke, K. B., Al-Mudhaffer, M., Sista, P., Kilcoyne, A. L. D., Stefan, M. C., Zhou, X., Dastoor, P. C., Belcher, W. J., (2015). "Probing the origin of photocurrent in nanoparticulate organic photovoltaics", *Sol. Energy Mater. Sol. Cells*, 140: 412-421.
52. Knickerbocker, B. M., Pesheck, C. V., Davis, H. T., Scriven, L. E., (1982). "Patterns of three-liquid-phase behavior illustrated by alcohol-hydrocarbon-water-salt mixtures", *J. Phys. Chem.*, 86: 393-400.
53. Washburn, N. R., Lodge, T. P., Bates, F. S., (2000). "Ternary polymer blends as model surfactant systems", *J. Phys. Chem. B*, 104: 6987-6997.
54. Sivula, K., Ball, Z. T., Watanabe, N., Frechet, J. M., (2006). "Amphiphilic diblock copolymer compatibilizers and their effect on the morphology and performance of polythiophene: fullerene solar cells", *J. Adv. Mater.*, 18: 206-210.
55. Tsai, J. H., Lai, Y. C., Higashihara, T., Lin, C. J., Ueda, M., Chen, W. C., (2010). "Enhancement of P3HT/PCBM photovoltaic efficiency using the surfactant of triblock copolymer containing poly(3-hexylthiophene) and poly(4-vinyltriphenylamine) segments", *Macromolecules*, 43: 6085-6091.

56. Chen, J., Yu, X., Hong, K., Messman, J. M., Pickel, D. L., Xiao, K., Dadmun, M. D., Mays, J. W., Rondinone, A. J., Sumpter, B. G., Kilbey, S. M., (2012). "Ternary behavior and systematic nanoscale manipulation of domain structures in P3HT/PCBM/P3HT-b-PEO films", *J. Mater. Chem.,* 22: 13013-13022.
57. Gu, Z. J., Kanto, T., Tsuchiya, K., Shimomura, T., Ogino, K., (2011). "Annealing effect on performance and morphology of photovoltaic devices based on poly (3-hexylthiophene)-b-poly (ethylene oxide)", *J. Polym. Sci., Part A: Polym. Chem.,* 49: 2645-2652.
58. Li, F., Shi, Y., Yuan, K., Chen, Y., (2013). "Fine dispersion and self-assembly of ZnO nanoparticles driven by P3HT-b-PEO diblocks for improvement of hybrid solar cells performance", *New J. Chem.,* 37: 195-203.
59. Maeda, Y., Shimoi, Y., Ogino, K., (2005). "Fabrication of microporous films utilizing amphiphilic block copolymers and their use as templates in poly (aniline) preparation", *Polym. Bull.,* 53: 315-321.
60. Gu, Z., Tan, Y., Tsuchiya, K., Shimomura, T.; Ogino, K., (2011). "Synthesis and characterization of poly (3-hexylthiophene)-b-polystyrene for photovoltaic application", *Polymers,* 3: 558-570.
61. Li, Q., Bao, Y., Wang, H., Du, F.; Li, Q., Jin, B., Bai. R., (2013). "A facile and highly efficient strategy for esterification of poly (meth) acrylic acid with halogenated compounds at room temperature promoted by 1, 1, 3, 3-tetramethylguanidine", *Polymer Chemistry,* 4: 2891-2897.
62. Iovu, M. C., Sheina, E. E., Gil, R. R., McCullough, R. D., (2005). "Experimental evidence for the quasi-"living" nature of the grignard metathesis method for the synthesis of regioregular poly (3-alkylthiophenes)", *Macromolecule,* 38: 8649-8656.
63. Xu, W. L., Zheng, F., He, J. L., Zhu, M. Q., Hao, X. T., (2015). "Quantifying phase separation and interfacial area in organic photovoltaic bulk heterojunction processed with solvent additives", *Chem. Phys.,* 457: 7-12.